JACS Au
AN OPEN ACCESS JOURNAL OF THE AMERICAN CHEMICAL SOCIETY

pubs.acs.org/jacsau

Article

Self-Assembly of Matchstick-Shaped Inorganic Nano-Surfactants with Controlled Surface Amphiphilicity

Da Hwi Gu, Wooyong Choi, and Jae Sung Son*

Cite This: *JACS Au* 2022, 2, 2307−2315

Read Online

ACCESS | Metrics & More | Article Recommendations | Supporting Information

ABSTRACT: Molecular and nanoscale amphiphiles have been extensively studied as building blocks for organizing macroscopic matter through specific and local interactions. Among various amphiphiles, inorganic Janus nanoparticles have attracted a lot of attention owing to their ability to impart multifunctionalities, although the programmability to achieve complicated self-assembly remains a challenge. Here, we synthesized matchstick-shaped Janus nano-surfactants that mimic organic surfactant molecules and studied their programmable self-assembly. High amphiphilicity was achieved through the hard−soft acid−base-based ligand-exchange reaction with strong selectivity on the surface of nano-matchsticks consisting of Ag_2S heads and CdS stems. The obtained nano-surfactants spontaneously assembled into diverse ordered structures such as lamellar, curved, wrinkled, cylindrical, and micellar structures depending on the vertical asymmetry and the interfacial tension controlled by their geometry and surface ligands. The correlation between the phase selectivity of suprastructures and the characteristics of nano-surfactants is discussed. This study realized the molecular amphiphile-like programmability of inorganic Janus nanostructures in self-assembly with the precise control on the surface chemistry.

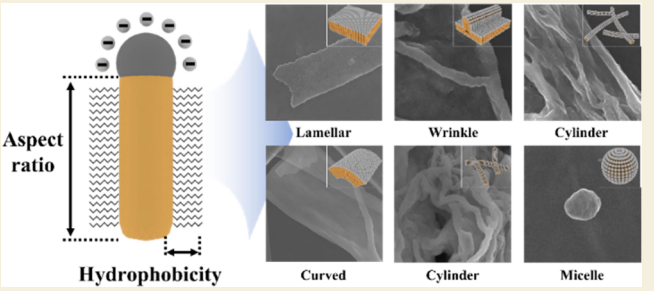

KEYWORDS: *nano-matchstick, nano-surfactants, self-assembly, inorganic ligands*

INTRODUCTION

Colloidal self-assembly of molecular building blocks is a critical process for organizing matter from the microscopic to the macroscopic scale.[1−6] For example, the self-assembly of asymmetric molecular amphiphiles, such as lipids, surfactants, and block copolymers composed of hydrophilic and hydrophobic segments, forms a variety of ordered suprastructures, where the targeted structures are programmable with building blocks' various parameters such as geometrical asymmetry, interfacial tension, and so forth.[7−10] Recently, by analogy with molecular amphiphiles, inorganic nanoparticles with Janus geometry have been regarded as a new type of nanoscale amphiphiles.[11−14] Due to their asymmetry, Janus nanoparticles can form self-assembled structures that are difficult to achieve with homogeneous or symmetric particles. Moreover, Janus nanoparticles can combine a variety of functional properties ranging from different types of magnetic, optical, and catalytic properties.[15−20] The controlled amphiphilicity and geometry of these particles, which determine the achievable degree of asymmetry, are essential in mediating their interactions and thus exploiting programmable self-assembly.[21−23] For example, depending on the geometrical hydrophilic−hydrophobic balance, snowman-shaped dumbbell nanoparticles were observed to form a range of self-assembled structures such as micelles and lamellar structures of different sizes. However, despite significant progress over the past decade, the colloidal self-assembly of inorganic Janus nanoparticles remains far less versatile than that of molecular amphiphiles in terms of dimensionality and programmability. This limitation may originate from underlying challenges in nanoparticle chemistry. For example, the synthesis of Janus nanoparticles has been limited to spheres or snowman-shaped dumbbells, which have a low packing density and lower asymmetry. In snowman-shaped Janus nanoparticles, the selective growth of one spherical lobe can cause destabilization and agglomeration of the nanoparticles, limiting the achievable asymmetry.[24] Moreover, amphiphilicity in the nanoparticles is generally achieved with the selective exposure of compartmentalized surfaces or selective ligand exchange with the organic surface agents of ionic polymers or charged hydrocarbons,[21−23] which sometimes lead to lower amphiphilicity or undesired collective interactions induced by ligands.[25] Recently, the tipped nanorods have been used as building blocks with a high aspect ratio for the self-assembly.[26,27] Zhao et al. reported the

Received: June 2, 2022
Revised: August 10, 2022
Accepted: August 30, 2022
Published: September 12, 2022

side-by-side self-assembly of Au-tipped CdSe nanorods and the resulting vertical closed-packed arrays.[26]

In this work, we present a design strategy for organic surfactant-mimetic matchstick-shaped inorganic nano-surfactants and their self-assembly into diverse types of structures. A developed ligand-exchange process based on the hard−soft acid−base (HSAB) theory[28−30] enabled selective exchange of surface ligands on the head of nanoscale "matchsticks" with inorganic anions[31−35] while preserving the long-chain organic ligands of the stem of the matchsticks. This results in matchstick-shaped nano-surfactants consisting of an ionic head and a long hydrophobic stem. These surfactants with high amphiphilicity easily form liquid droplets in nonpolar/polar phases. They also assemble into a variety of structures with extremely high lateral packing densities, such as lamellar, curved, wrinkled, cylindrical, and micellar structures, all of which are modulated by the controlled vertical asymmetry and interfacial tension of the nano-surfactants. The creation of ordered structures by surfactant assembly is discussed based on the curvature of self-assemblies with parameters of the building blocks. Overall, this study demonstrates the molecular amphiphile-like programmability of Janus nanoparticle self-assembly.

RESULTS AND DISCUSSION

Synthesis of Organic Surfactant-Mimetic Ag_2S−CdS Nano-Surfactants

The inorganic nano-surfactants were synthesized by selective ligand exchange on Ag_2S−CdS heterostructured nano-matchsticks (Figure 1a). Each organic surfactant-mimetic nano-matchstick consisted of a Ag_2S spherical head and a long CdS stem. This model system was selected because of its overall chemical stability and the distinct surface reactivity between the Ag_2S head and CdS stem.[36] The nanostructure was synthesized using the seed-mediated growth method (Figures S1−S3), where the Ag_2S seed nanoparticles were synthesized first and then the CdS stems were grown on the Ag_2S seeds. Transmission electron microscopy (TEM) images show matchstick-shaped nanostructures comprising spherical Ag_2S heads with a size of 10 nm and rod-shaped CdS stems with a diameter of 9 nm (Figure 1b). The aspect ratio of nano-matchsticks ranged from 2 to 10. The absorption spectrum of these nano-matchsticks (Figure S3) shows a broad absorption in the visible to UV range, due to the indirect band gap of 2.25 eV of Ag_2S nanoparticles and an excitonic peak at 480 nm, which agrees with the absorption spectrum of CdS nanorods with a similar diameter.[36]

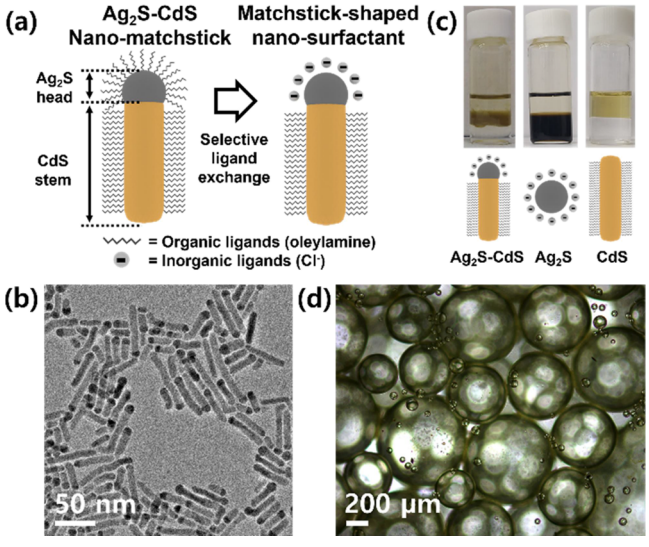

Figure 1. (a) Schematic illustration of synthesis of nano-matchstick and matchstick-shaped nano-surfactants. (b) TEM images of oleylamine-capped Ag_2S−CdS nano-matchsticks. (c) Photographs and illustrated models of the Cl^-/oleylamine-capped Ag_2S−CdS matchstick-shaped nano-surfactants (left), Cl^--capped Ag_2S nanoparticles (middle), and oleylamine-capped CdS stems (right). (d) Optical microscopy image of droplets coated with Cl^-/oleylamine-capped Ag_2S−CdS matchstick-shaped nano-surfactants in dichlorobenzene/ethylene glycol and DI water after vortexing for 1 min.

To realize amphiphilicity in the nano-surfactants, a selective ligand-exchange reaction was designed based on the HSAB theory.[28−30] This theory sorts Lewis acids and bases into "soft" and "hard" classes using the criterion of hardness (i.e., their polarizability) and assumes that Lewis acids tend to form stable complexes with Lewis bases of comparable hardness. Since the hardness of Cl^- anions ($\eta \sim 4.7$) is more comparable to Ag^+ cations ($\eta \sim 6.9$) than Cd^{2+} cations ($\eta \sim 10.3$),[28] we introduced the Ag_2S head-favored Cl^- anions to selectively replace the organic ligands on their surfaces by the two-phase ligand-exchange process. Thus, this process causes the selective exchange of oleylamine ligands capped on the Ag_2S head with Cl^- anions, while the identical organic ligands capped on the CdS stem are conserved. During the ligand-exchange reaction with Cl^- anions, the matchstick-shaped nano-surfactants were transferred to the interlayer between the nonpolar hexane and polar *N*-methylformamide (NMF) phases due to the amphiphilic motif (Figure 1c, left). For comparison, we conducted the same ligand-exchange reaction using isolated Ag_2S nanoparticles and CdS nanorods. The Ag_2S nanoparticles were fully transferred to the polar NMF phase after ligand exchange with Cl^- anions (Figure 1c, middle), whereas the CdS nanorods (Figure S1b) remained in the nonpolar hexane phase (Figure 1c, right). The negative ζ-potential value of −29 mV further supports the Cl^- capping on the surfaces of Ag_2S nanoparticles (Figure S4). Additionally, the ligand exchange of Ag_2S nanoparticles with Cl^- was further confirmed by the control experiments, in which the two-phase reaction of oleylamine-capped Ag_2S nanoparticles in the absence of Cl^- ion was conducted. In this reaction, Ag_2S nanoparticles were not transferred from the nonpolar to polar phase (Figure S5). Accordingly, we could rule out the possibility that the ligand-exchange reaction causes the formation of the naked Ag_2S nanoparticles with negative surface charges by the removal of oleylamine ligands.

The degree of ligand exchange was estimated using Fourier transform infrared (FT-IR) absorption spectroscopy (Figure S6). For Ag_2S nanoparticles, the absence of a peak near 2800 cm^{-1} indexed to the C−H stretching modes indicated the complete removal of oleylamine, whereas this peak was well conserved for CdS nanorods after the ligand-exchange reaction. The Ag_2S−CdS nano-surfactants showed a reduced peak intensity at this position. These results demonstrate selectivity of the HSAB-based ligand-exchange reaction to obtain amphiphilic Ag_2S−CdS matchstick surfactants.

The emulsification behavior of Ag_2S−CdS surfactants was investigated in terms of droplet formation and stability (Figures 1d, S7 and S8).[37−40] The optical microscopy (OM) image (Figure S7a) shows that nano-surfactants in the hexane/

https://doi.org/10.1021/jacsau.2c00333
JACS Au 2022, 2, 2307−2315

NMF system easily formed a Pickering emulsion, which remained stable for more than a minute. With the less volatile solvent combination of dichlorobenzene/ethylene glycol and DI water, the formed droplets remained for several hours (Figures 1d and S8). However, neither Ag_2S nanoparticles nor CdS nanorods alone could create stable droplets (Figure S7b–d) under both conditions. These results demonstrate the surface activity of the nano-matchstick surfactants.

Self-Assembly of Ag_2S–CdS Nano-Surfactants with Controllable Asymmetry

In organic amphiphiles, the length of the hydrophobic segment is a major parameter for programming their self-assembly. Similarly, we investigated the self-assembly of matchstick-shaped inorganic nano-surfactants by controlling the length of their hydrophobic stem, which in turn controls both the vertical asymmetry and the hydrophilic/hydrophobic balance. To this end, we carried out a size selection process to classify the Ag_2S–CdS nano-matchsticks by their aspect ratios (Figure 2). Shorter nano-matchsticks (i.e., those with a smaller aspect ratio) displayed a weaker relative absorbance of the CdS stem at 480 nm, while the broad spectral tail at higher wavelengths originating from the Ag_2S head increased (Figure S9).

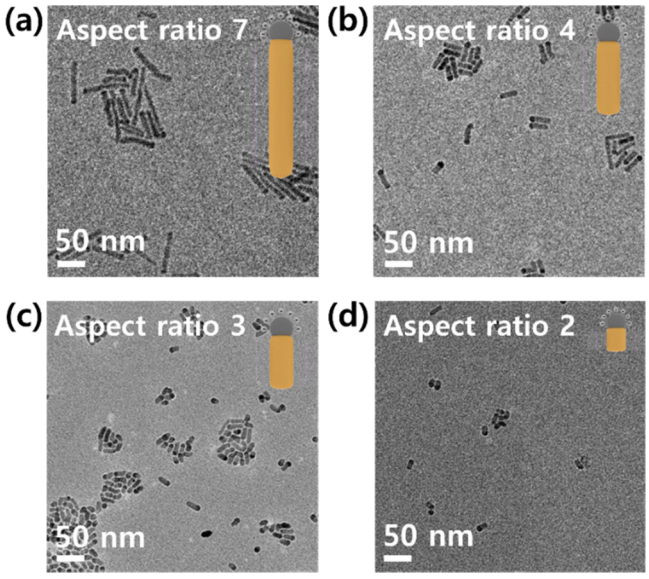

Figure 2. TEM images of oleylamine-capped nano-matchsticks of aspect ratios of (a) 7, (b) 4, (c) 3, and (d) 2.

To investigate the nano-matchsticks' ability to form ordered structures by self-assembly, we conducted experiments using nano-matchsticks with selected aspect ratios ranging from 2 to 7, outside of which ordered self-assemblies were not formed. (Figure S10). The self-assembly experiments were conducted by dispersing the amphiphilic building blocks in a polar (NMF) medium since it was known as one of the most polar solvents (dielectric constant (ε) = 167.8) and affordable for the dispersion of inorganic ligand-capped nanoparticles.[32] To investigate the solvent effect, we conducted the self-assembly of the nano-surfactants with the aspect ratio of 5–7 in different polar solvents of dimethylformamide (ε = 37.51) and water (ε = 80.4). As shown in TEM images (Figure S11), we could not observe any ordered structures.

The assembly process of the nano-surfactants was completed within 10 minutes. As shown in TEM images (Figure S12a,b), the self-assemblies of the nano-surfactants aged for 10 min and 24 h were identical in microstructures. Moreover, the dynamic light scattering (DLS) analysis (Figure S13) on the dispersed self-assemblies shows that the size of structures was on the scale of several micrometers, and it was not changed after 24 h, indicating that the macrostructures were not changed as well. Also, this result suggests that the nano-surfactants were assembled at the dispersed phase in NMF before the post-drying for the sample preparation. We further investigated the time evolution of the colloidal stability of these self-assemblies. The suspension maintained the stability for an hour but started to settle down at 2 h and was wholly sedimented at 5 h (Figure S14). This sedimentation should be attributed to their relatively large sizes.

When the aspect ratio was 5–7, typical lamellar structures were formed. The top view scanning electron microscopy (SEM) image shows a rectangular microplate with lateral sizes of several micrometers (Figure 3a). The top view TEM image reveals that the nano-surfactants are close-packed with short-range hexagonal ordering (Figure 3b). The cross-sectional TEM clearly indicates the homogeneously assembled double bilayers of planar lamellar structures (Figures 3c,d and S15a), which further confirms lateral assembly of the matchstick-shaped nano-surfactants. Moreover, the hydrophilic Ag_2S heads, which appear in the TEM images as areas with darker contrast compared to the CdS stems, point toward the surfaces of the lamellar structure because of the polar NMF

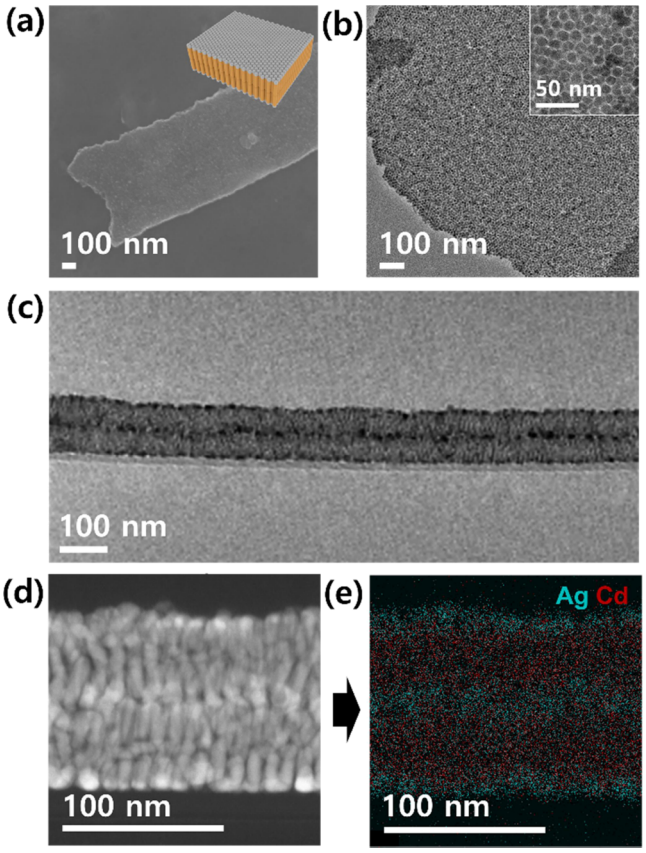

Figure 3. (a) SEM image, (b) TEM image, cross-sectional (c) TEM image, (d) STEM image, and (e) elemental mapping image of the lamellar structured self-assembly of matchstick-shaped nano-surfactants. The inset in (b) is a magnified TEM image.

https://doi.org/10.1021/jacsau.2c00333
JACS Au 2022, 2, 2307–2315

environment. The orientation of the nano-matchsticks was also investigated using energy-dispersive X-ray spectroscopy (EDS). Elemental mapping results of the cross-sectional scanning TEM (STEM) image clearly show that the heads are oriented toward the outside (Figure 3e). In addition, TEM images of the lamellar structures at different tilt angles reveal that the edges of the lamellar structures are encased by laterally aligned matchstick-shaped nano-surfactants without rolling or bending (Figure S16). Although most of the lamellar structures consisted of double bilayers, we also observed the formation of single and triple bilayers (Figure S15b–d). Also, the slipping or delamination of the bilayer was also observed, which can be responsible for the wrinkling of the single bilayer in the shorter aspect ratio of the nano-surfactants.

When the aspect ratio decreases to 4, the lamellar structures start to curve. In the top view TEM image, the basal plane of the lamellar structure is well formed, while the matchsticks gradually lie at the edge of the structure (Figure S17). This is in contrast to the lamellar structure formed from the matchstick-shaped nano-surfactants with a higher aspect ratio, and the TEM image reveals that the matchsticks at the edges are aligned and point to the top (Figure 3b). When the aspect ratio is further reduced to 3, the lamellae become more curved and eventually form wrinkled structures. The radius of curvature for the wrinkles ranges from around one hundred to several hundred nanometers (Figure 4a). Moreover, the TEM image, lateral view STEM, and elemental mapping show that the wrinkles of suprastructures are constructed by the curved lamellae (Figures 4b–d and S15e). Finally, at the aspect ratio of 2 (the minimum value required to form ordered assembled structures), the wrinkles turn into interconnected cylinders, indicating stronger curving in the lamellae (Figure 4e,f). Randomly created numerous wrinkles in the lamellar structures might be transformed to cylinders by decreasing the radius of curvature during the assembly process, as a result, leading to the formation of interconnected cylinders. SEM and TEM images show that cylinders with the diameters ranging from 100 to 200 nm are interconnected together. Especially, the void spaces among the interconnected cylinders are clearly observed in the TEM image (Figure 4f). This is in contrast to that of the wrinkled structures, which have the basal plane of lamellar structures between wrinkles (Figure 4b). This result suggests that most lamellae formed the rolled cylinders in this structure. These findings show that the geometric asymmetry of matchstick-shaped surfactants has a significant impact on the overall morphology of the self-assembled structure, with stronger bending at smaller aspect ratios.

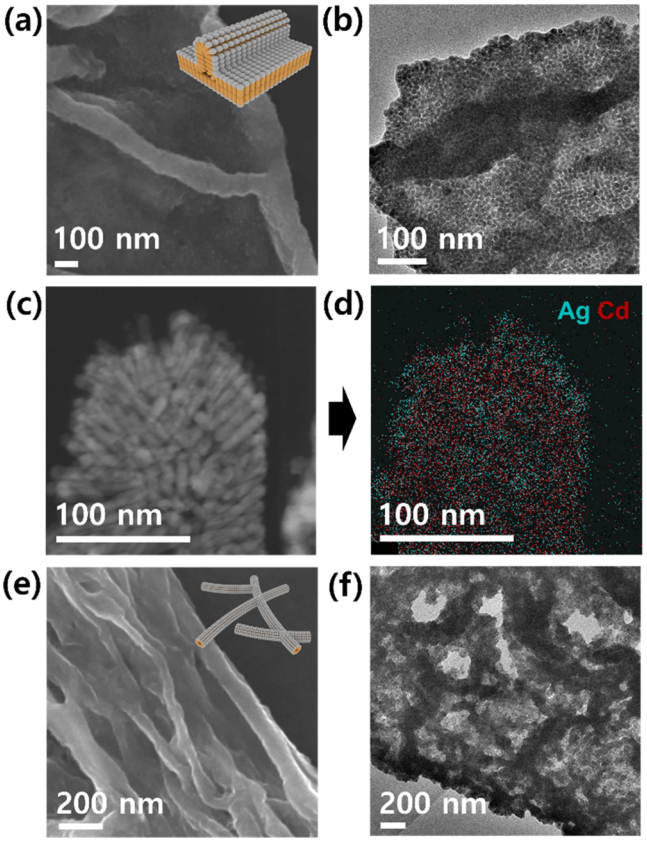

Figure 4. (a) SEM image, (b) TEM image, (c) STEM image, and (d) elemental mapping image of the wrinkle-structured self-assembly. (e) SEM image and (f) TEM image of the cylinder-structured self-assembly.

Self-Assembly of Ag_2S–CdS Nano-Surfactants with Controllable Interfacial Tension

The interfacial tension between the building blocks and the medium is the primary driving force in the self-assembly of colloids. To control the degree of incompatibility between the nano-surfactants and the solvent, we varied the chain length of the organic capping ligands on the CdS stem to tune its hydrophobicity and interfacial tension with the polar NMF solvent (Figure 5a). To this end, the primary oleylamine (C18) ligands were exchanged with shorter alkylamines. Ordered assemblies were formed when the hydrocarbon was C12 (dodecylamine) or longer, while alkylamines with shorter hydrocarbon chains resulted in disordered structures (Figure S18) because the interfacial tension between the short alkylamines and the polar solvent was not high enough to drive the assembly spontaneously. The colloidal stability of the matchsticks was retained for all studied nano-surfactants of alkylamine ligands (C12~C18) (Figure S19a). Ligand exchange on the nano-matchsticks was further confirmed using ^{1}H nuclear magnetic resonance (NMR) spectroscopy (Figure S19b). The NMR spectra clearly show that, after exchange with other saturated alkylamines, the peak at 5.4 ppm (C═C bonding of oleylamine) disappeared, indicating complete ligand exchange.

As mentioned above, the nano-surfactant with oleylamine (C18)-capped stems self-assembled into flat lamellar structures (Figure 3). After decreasing the chain length of alkylamine to C16 (hexadecylamine), the nano-surfactant formed the curved lamellar structures. The SEM image (Figure 5b,c) shows the large-sized wrinkled lamellar structures, of which wrinkles have the radius of curvature of larger than 1 μm. Interestingly, in some suprastructures, we observed that the formation of the free-standing rolled lamellae with similar curvatures to wrinkles (Figure 5d). The TEM image shows that the contrast gradually becomes darker from the center to the edge, indicating that the nano-surfactants gradually lie at edge of the structure, which was further confirmed by the HRTEM image (the inset of Figure 5d). After decreasing the chain length of alkylamine to C14 (tetradecylamine), the nano-surfactant formed interconnected cylindrical structures with the radius of curvatures ranging from around one hundred to several hundred nanometers (Figure 5e–g), which was smaller than those of the structure obtained from C16-nano-suractants. Rather, the

https://doi.org/10.1021/jacsau.2c00333
JACS Au 2022, 2, 2307–2315

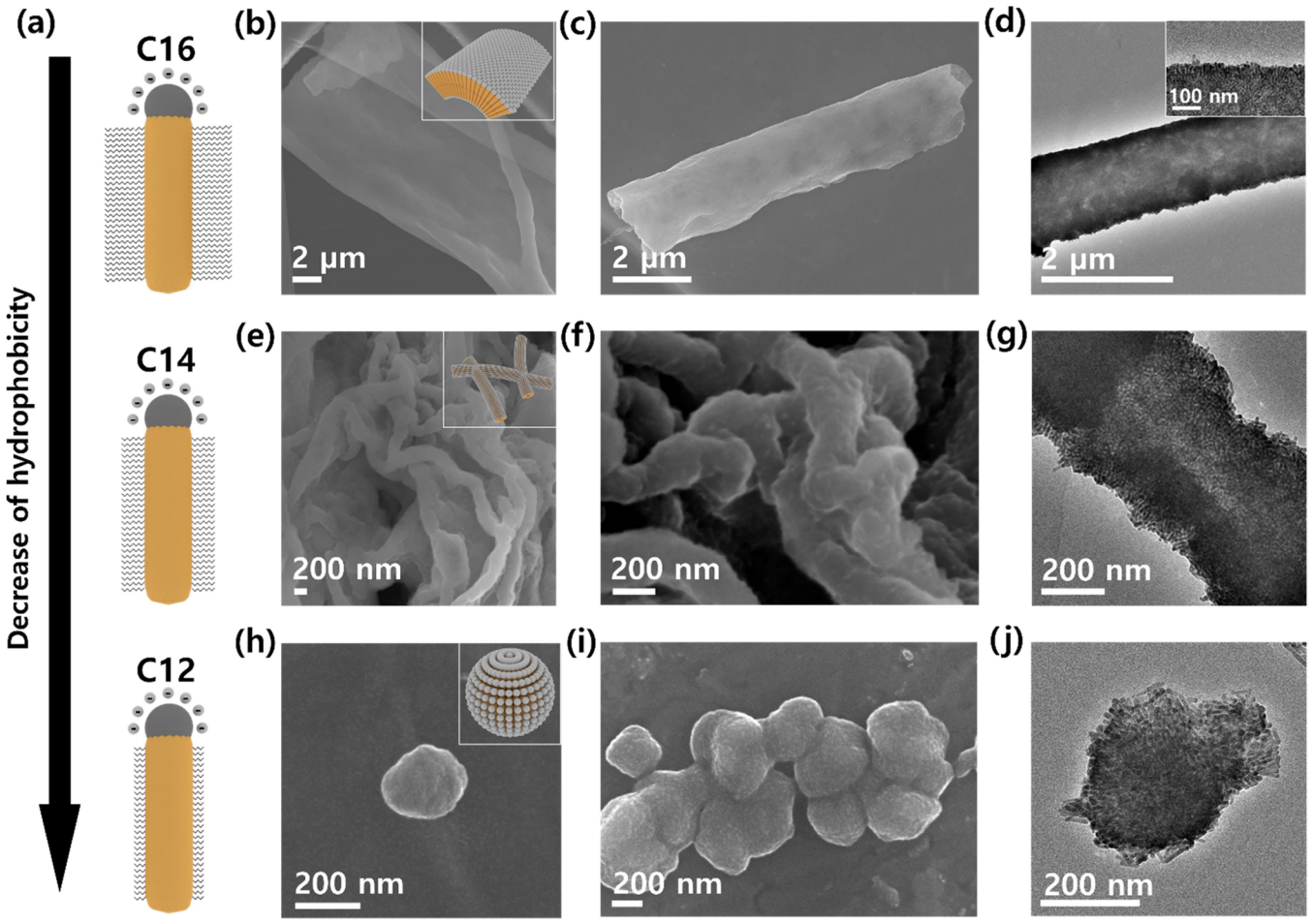

Figure 5. (a) Illustrated models of the matchstick-shaped nano-surfactants capped with oleylamine (top), tetradecylamine (middle), and dodecylamine (bottom). (b,c) SEM images and (d) TEM image of the self-assembly of Cl^-/hexadecylamine-capped matchstick-shaped nano-surfactants. The inset in (d) is a magnified TEM image. (e,f) SEM images and (g) TEM image of the self-assembly of Cl^-/tetradecylamine-capped matchstick-shaped nano-surfactants. (h,i) SEM images and (j) TEM image of the self-assembly of Cl^-/dodecylamine-capped matchstick-shaped nano-surfactants.

overall morphology and curvatures were very similar to those observed in the self-assemblies of the nano-surfactants with an aspect ratio of 2. As shown in the TEM image, the matchsticks stand upright in the center of the cylinder, but progressively tilt toward the edge, eventually lying down at the edge of the structure, demonstrating the cylindrical structure. More interestingly, upon further decreasing the hydrocarbon chain length to C12, spherical micellar structures were formed by self-assembly (Figure 5h–j). The SEM image (Figure 5h) reveal that the micelles are free-standing, and that their sizes (100 to 300 nm) are smaller than the diameters of curvature observed in other curved self-assembles. Some micelles are merged into multiple micellar clusters (Figure 5i). This clustering could be induced by the adhesive collisions and followed fusions of micelles. Similar phenomena of clustering of micellar structures have been reported in the self-assembly of block co-polymers.[41] The TEM images (Figure 5j) show that the nano-surfactants are well aligned laterally and are progressively tilted toward the edge, agreeing with the typical micellar assembly of organic amphiphiles. Nano-surfactants were well aligned laterally along the curved direction. This is in stark contrast to the random agglomeration of nano-surfactants that were usually observed in the samples collected under different conditions, as shown in the TEM image (Figure S20).

These self-assemblies depending on the hydrophobicity of nano-surfactants indicate that the bending of self-assemblies became more intensified with lower hydrophobicity owing to a lower incompatibility of the matchsticks with the medium.

Phase Selectivity and Uniformity of Self-Assemblies

The matchstick-shaped nano-surfactants here were designed to mimic molecular amphiphiles with a high vertical asymmetry. In particular, the current nano-surfactants have many similarities to block copolymers in terms of amphiphilicity and diverse ordered self-assemblies. The morphology of self-assemblies formed by block copolymers is generally dictated by the bending energy, which has been well established by the following relationship:

$$\Delta E_C \propto \frac{\gamma d^2}{R^2} \propto \gamma \Delta a \tag{1}$$

where ΔE_C is the free energy penalty per chain, γ is the interfacial tension between the hydrophobic segments and the solvent, d is the thickness of the membrane, R is the radius of curvature, and Δa is the exposed area.[42−44] The equilibrium morphology of self-assembled suprastructures is determined by both the mixing entropy (driving the formation of many assemblies) and molar bending energy (driving the formation

https://doi.org/10.1021/jacsau.2c00333
JACS Au 2022, 2, 2307−2315

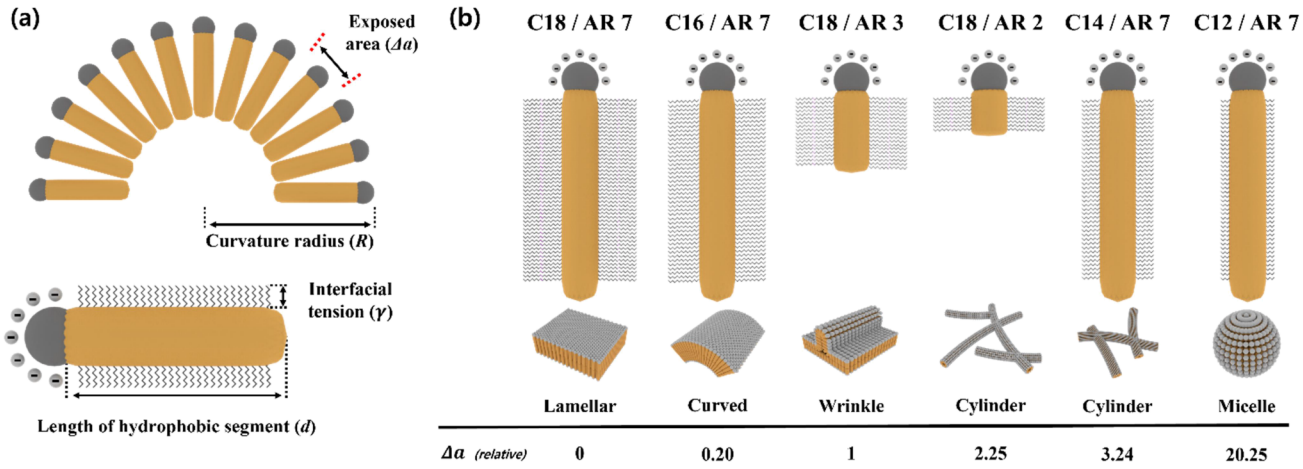

Figure 6. (a) Parameters affecting the interfacial energy of the matchstick-shaped nano-surfactants. (b) Illustrated models of matchstick-shaped nano-surfactants and resulting self-assembly structure of different conditions with Δa.

of a small number of assemblies), which jointly determine ΔE_C. Accordingly, the given values of ΔE_C, γ, and d are thermodynamically balanced with the curvature of the self-assemblies, further determining Δa.

We controlled the length and surface hydrophobicity of the hydrophobic stem of the nano-surfactants, thereby modulating the vertical geometry and interfacial tension (Figure 6a). When the lamellar phase of the self-assembly transforms into curved structures, such as cylinders and micelles, the free energy change can be understood by the identical relationship. The controlled length and surface hydrophobicity of the nano-surfactants define d and γ in the formed self-assemblies. Systematically decreasing the length of the hydrophobic segment reduces d, resulting in a smaller radius of curvature R for the self-assemblies. This decrease can lead to a phase transition from lamellae to wrinkles and interconnected cylinders. In addition, the reduced hydrophobicity after capping the surface with shorter hydrocarbon ligands decreases γ by providing less compatibility with the polar solvent medium. This is further supported by previous reports[45−47] where the oleyl group (C18) exhibited a surface tension in polar solvent 1.05, 1.1, and 1.2 times larger than those of hexadecyl, tetradecyl, and dodecyl groups. This decrease in γ of the nano-surfactants reduces R, which explains the phase transition from the lamellar structure to cylinders and micelles. Based on the experimentally characterized d and R, we estimated Δa for the obtained curved self-assemblies. The Δa values in Figure 4 were calculated using eq 1. The R of the self-assembly was measured using the TEM image of the assembled structures, and the detailed structural parameters are listed in Table S1. For easier comparison, the Δa value of C18/AR3 (aspect ratio) was defined as 1 and Δa values of other conditions were normalized. Owing to the infinite R, the lamellar structure has 0 of Δa in the calculation, though Δa in these structures should be minimum, compared with other self-assemblies. In the curved self-assemblies, the Δa values increased in the order of curved, wrinkled, cylindrical, and micellar structures. Although the curved structure has a minimal Δa of 0.2, that of the wrinkled structure considerably increased to 1. The Δa values of the two cylindrical structures (C18 with an aspect ratio of 2 and C14 with an aspect ratio of 7) obtained under different conditions are very similar, while that of micelle structures (C12 with an aspect ratio of 7) is significantly increased (Figure 6b) to indicate higher curvatures. Overall, the Δa values of all these structures have remarkably distinct, well distinguishing the corresponding curved self-assemblies with different curvatures. This result is in line with the behaviors of molecular amphiphiles like block copolymers,[42] showing the potential of the programmability of curved self-assemblies with parameters of Janus inorganic nano-surfactants.

There can be two strategies to improve the uniformity of the self-assemblies. First, the uniformity of building blocks in sizes, shapes, and surface states can improve the uniformity of resulting self-assemblies. As seen in this study, the aspect ratio and surface states of the nano-surfactants play critical roles in determining the phases and morphologies in the self-assemblies. The structural uniformity of the nano-surfactants in this study can be improved by the synthetic advances for Ag_2S−CdS nano-matchsticks since the as-synthesized matchsticks have broad distributions in their lateral dimensions. Although the size selection significantly narrowed the distribution, there is still variation observed. More importantly, the uniformity in the surface state is more difficult to be secured in the nano-surfactants. For example, we sometimes observed the undesired precipitation of nanoparticles during the purification process, which can be attributed to the desorption of oleylamine ligands. This phenomenon could deteriorate the uniformity of the surface states of nanoparticles.

Second, the slow self-assembly of the nano-surfactants can improve the uniformity of the self-assembled structures. In this study, the self-assembly of nano-surfactants is relatively rapid and completed within 10 min. This fast self-assembly could kinetically affect the final structures rather than the thermodynamic process, so sometimes unwanted merging or interconnection of structures was observed. Dischler et al. reported the morphology transition of block copolymer assembly with the slow and controlled changes in the solvent polarity, generating uniform and selective self-assemblies.[42] Such controlled kinetics in the self-assembly achieved by the process can improve the uniformity of the self-assemblies of nano-surfactants in this study.

CONCLUSIONS

We designed a selective HSAB ligand-exchange reaction to synthesize organic surfactant-mimetic matchstick-shaped nano-surfactants with high amphiphilicity. By carefully engineering

https://doi.org/10.1021/jacsau.2c00333
JACS Au 2022, 2, 2307−2315

the nano-surfactant's geometry and surface state, diverse macroscopic suprastructures (flat, curved, wrinkled lamellar, cylindrical, and micellar) were formed by self-assembly. These suprastructures were further discussed in terms of the curvatures of self-assemblies and geometry and interfacial tension of individual nano-matchsticks. Our approach imparts molecular amphiphile-level programmability to inorganic nanoparticles, unveiling a new way to target complicated self-assembled structures with macroscopic order. Moreover, our design strategy can be extended to other classes of functional inorganic hybrid nanoparticles such as magnetic, luminescent, and plasmonic materials, which can provide multiple functionalities as well as structure-induced properties to the self-assembly. Surface stabilization, another prominent function of surfactants, was also observed in liquid droplets stabilized by these inorganic nano-surfactants, and this can also be extended to different macroscopic matters. We believe that such inorganic nano-surfactants are an ideal model system for understanding the fundamental self-assembly of amphiphiles.

MATERIALS AND METHODS

Materials

Silver nitrate ($AgNO_3$, ≥99%), oleic acid (OA, technical grade, 90%), oleylamine (OlAm, 70%), sulfur (S, 99.99%), cadmium acetylacetonate ($Cd(acac)_2$, ≥99.9%), trioctylphosphine (TOP, 90%), tetradecylamine (95%), dodecylamine (98%), decylamine (95%), octylamine (99%), heptylamine (99%), hexylamine (99%), and NMF (99%) were purchased from Sigma-Aldrich. KCl (99%), and ammonium carbonate ($(NH_4)_2CO_3$, 30%) were purchased from SAMCHUN Chemicals.

Characterization Methods and Instruments

TEM images at different tilt angles were obtained using a JEOL-2100 instrument operated at 200 kV. STEM images and elemental mapping images of the self-assembly were obtained using EDS with a JEM-2100F, JEOL instrument. FT-IR spectra were obtained using a 670/620 Varian FT-IR spectrometer in the transmission mode. SEM images were obtained using an SU7000 FE-SEM instrument (Hitachi High-Tech) operated at 20 kV. NMR measurements were performed on a 400 MHz NMR AVANCE III HD Console (Bruker). OM images were obtained using an Olympus BX51M microscope. UV−vis absorption spectra were recorded using a Shimadzu UV-2600 spectrophotometer. ζ-Potential data and DLS data were collected using a Nano-ZS of Malvern instrument.

Synthesis of Seed Nanoparticles

Ag_2S seed nanoparticles (10 nm) were synthesized following the report by Dong et al. with slight modification.[36] $AgNO_3$ (1 mmol), OA (0.5 mL), and OlAm (20 mL) were put into a three-necked round-bottom flask. The mixture was heated to 180 °C for 30 min under vacuum and reacted for 1 h under a N_2 atmosphere. After aging for 1 h, the solution was cooled to 100 °C, and a sulfur solution (1 mmol of S dissolved in 3 mL of toluene) was injected and further stirred for 5 min. The reaction mixture was cooled to room temperature (RT). The synthesized Ag_2S seed nanoparticles were washed with excess ethanol and re-dispersed in chloroform (10 mL).

Synthesis of Nano-Matchsticks

Ag_2S−CdS nano-matchsticks were synthesized following the method reported by Dong et al. with slight modification.[36] Ag_2S seed nanoparticles (12 mg/mL, 1 mL), $Cd(acac)_2$ (0.2 mmol), OA (2 mL), and OlAm (10 mL) were put into a three-necked round-bottom flask under a N_2 atmosphere. After degassing under vacuum for 1 h, the mixture was heated to 140 °C under a N_2 atmosphere. Then, a sulfur solution (0.2 mmol of S dissolved in 2 mL of OlAm) was slowly injected using a syringe pump over 1 h and further stirred for 1 h at 140 °C. The reaction mixture was cooled to RT and washed with excess ethanol. The precipitates were dispersed in hexane (10 mL). To saturate the OlAm capping, the synthesized nano-matchsticks were stirred with excess OlAm before size selection. Specifically, Ag_2S−CdS nano-matchsticks (1 mL), hexane (5 mL), and OlAm (1 mL) were placed in a 10-mL vial and stirred vigorously overnight. The reaction mixture was washed with excess ethanol and re-dispersed in hexane (1 mL).

Nano-matchsticks with aspect ratios larger than 10 were synthesized by the same procedure as described above, but with a smaller amount of Ag_2S seed nanoparticles (0.5 instead of 1 mL).

Preparation of CdS Stems

Separated CdS stems were prepared following the method reported by Dong et al. with slight modification.[36] The Ag_2S heads were removed from Ag_2S−CdS nano-matchsticks to investigate the independent surface reactivity of CdS stems. The as-synthesized nano-matchsticks (1 mL) were combined with OA (2 mL) and OlAm (10 mL) in a three-necked round-bottom flask. The mixture was degassed under vacuum for 1 h and heated to 160 °C under a N_2 atmosphere. TOP (10 mL) was injected into the reaction mixture and further reacted for more than 10 h until the color turned yellow. After aging overnight at 160 °C, the reaction mixture was cooled to RT and then washed with excess ethanol. The precipitate was re-dispersed in hexane.

Size Selection Process

Size selection of the Ag_2S−CdS nano-matchsticks was carried out by controlling the acetone content during the centrifugation process. First, Ag_2S−CdS solution in hexane (1 mL) was added with acetone (0.1 mL) and centrifuged at 7500 RPM. After separation from the precipitates, the supernatant was combined with 0.1 mL of acetone, followed by one more step of centrifugation at the same spinning rate. After each centrifugation, the precipitates were re-dispersed in 1 mL of hexane, and the supernatant was centrifuged at a higher antisolvent content. This procedure was repeated 10 times until the acetone content reached 1 mL.

Amine Exchange Process

After the size selection process, the types of amine on the nano-matchsticks could be further varied with the amine exchange process. Ag_2S−CdS nano-matchsticks in hexane (5 mg/mL, 1 mL), additional hexane (1 mL), and an amine (0.5 mL) were stirred together overnight. The reaction mixture was then washed with excess ethanol and dispersed in hexane (1 mL). The used amines were oleylamine (18 carbons, C18), tetradecylamine (C14), dodecylamine (C12), decylamine (C10), octylamine (C8), heptylamine (C7), and hexylamine (C6).

Preparation and Self-Assembly of Nano-Surfactants

Matchstick-shaped nano-surfactants were prepared using a selective ligand-exchange process. The nano-matchsticks (1 mg in 1 mL hexane) and an inorganic ligand [KCl or $(NH_4)_2CO_3$, 5 mg, dissolved in 1 mL NMF] were blended with a vortex mixer for 1 min. After the selective ligand-exchange process, the nano-matchsticks were transferred to the interlayer between the hexane and NMF. The excess inorganic ligands and residual amines were removed by washing with isopropyl alcohol (1.5 mL). The resulting nano-surfactants were dispersed in 0.2 mL of NMF as a polar solvent.

The matchstick-shaped nano-surfactant assemblies were collected and aged on a carbon grid for several hours to form a thermodynamically stable structure. Then, the sample was fixed by vacuum drying before further characterization, because air-drying was not sufficient for removing solvents with high boiling points.

Droplet Stability of Nano-Surfactants

Surface activation of the matchstick-shaped nano-surfactants was carried out using combinations of nonpolar and polar liquid phases [e.g., hexane/NMF, dichlorobenzene/1:1 (v/v) mixtures of DI water and ethylene glycol].[23] A solution of the nano-surfactants in a nonpolar solvent (0.5 mg/mL, 0.5 mL) was combined with a polar solvent (0.5 mL) and agitated using a vortex mixer for 1 min (3000 RPM). This produced droplets with diameters of 200−500 μm measured with OM.

https://doi.org/10.1021/jacsau.2c00333
JACS Au 2022, 2, 2307−2315

■ ASSOCIATED CONTENT

Supporting Information

The Supporting Information is available free of charge at https://pubs.acs.org/doi/10.1021/jacsau.2c00333.

Photographs of vial containing nanoparticles, TEM, absorption spectra, FT-IR spectra, OM, and ^{1}H NMR (PDF)

■ AUTHOR INFORMATION

Corresponding Author

Jae Sung Son − *Department of Materials Science and Engineering and Graduate School of Semiconductor Materials and Devices, Ulsan National Institute of Science and Technology (UNIST), Ulsan 44919, Republic of Korea;* orcid.org/0000-0003-3498-9761; Email: jsson@unist.ac.kr

Authors

Da Hwi Gu − *Department of Materials Science and Engineering, Ulsan National Institute of Science and Technology (UNIST), Ulsan 44919, Republic of Korea*

Wooyong Choi − *Department of Materials Science and Engineering, Ulsan National Institute of Science and Technology (UNIST), Ulsan 44919, Republic of Korea*

Complete contact information is available at: https://pubs.acs.org/10.1021/jacsau.2c00333

Author Contributions

D.H.G., and J.S.S. designed the experiments, analyzed the data, and wrote the paper. D.H.G. carried out the synthesis and characterization of nano-matchsticks, and the basic characterization of the self-assembled structures. D.H.G., and W.C. performed the microstructural analysis of the self-assembled structures. All authors discussed the results and commented on the manuscript.

Notes

The authors declare no competing financial interest.

■ ACKNOWLEDGMENTS

We acknowledge the National Research Foundation Grants of Korea (NRF) funded by the Ministry of Science and ICT of Republic of Korea (NRF-2019R1A2C1087487; NRF-2018M3A7B8060697). D·H.G. was supported by the NRF grant funded by the Korean Government (NRF-2018H1A2A1062416)-Global Ph.D. Fellowship Program.

■ REFERENCES

(1) Boles, M. A.; Engel, M.; Talapin, D. V. Self-assembly of colloidal nanocrystals: From intricate structures to functional materials. *Chem. Rev.* **2016**, *116*, 11220−11289.

(2) Liu, Y.; Yao, D.; Zhang, H. Self-assembly driven aggregation-induced emission of copper nanoclusters: A novel technology for lighting. *ACS Appl. Mater. Interfaces* **2018**, *10*, 12071−12080.

(3) Kim, D.; Bae, W. K.; Kim, S.-H.; Lee, D. C. Depletion-mediated interfacial assembly of semiconductor nanorods. *Nano Lett.* **2019**, *19*, 963−970.

(4) Yang, S.-M.; Kim, S.-H.; Lim, J.-M.; Yi, G.-R. Synthesis and assembly of structured colloidal particles. *J. Mater. Chem.* **2008**, *18*, 2177−2190.

(5) Nie, Z.; Petukhova, A.; Kumacheva, E. Properties and emerging applications of self-assembled structures made from inorganic nanoparticles. *Nat. Nanotechnol.* **2010**, *5*, 15−25.

(6) Gu, D. H.; Lee, J.; Ban, H. W.; Lee, G.; Song, M.; Choi, W.; Baek, S.; Jeong, H.; Lee, S. Y.; Choi, Y.; Park, J.; Park, Y. I.; Son, J. S. Colloidal suprastructures self-organized from oppositely charged all-inorganic nanoparticles. *Chem. Mater.* **2020**, *32*, 8662−8671.

(7) Israelachvili, J. N.; Mitchell, D. J.; Ninham, B. W. Theory of self-assembly of lipid bilayers and vesicles. *Biochim. Biophys. Acta* **1977**, *470*, 185−201.

(8) Nagarajan, R. Molecular packing parameter and surfactant self-assembly: The neglected role of the surfactant tail. *Langmuir* **2002**, *18*, 31−38.

(9) Mai, Y.; Eisenberg, A. Self-assembly of block copolymers. *Chem. Soc. Rev.* **2012**, *41*, 5969−5985.

(10) Malenfant, P. R. L.; Wan, J.; Taylor, S. T.; Manoharan, M. Self-assembly of an organic−inorganic block copolymer for nano-ordered ceramics. *Nat. Nanotechnol.* **2007**, *2*, 43−46.

(11) Jiang, S.; Chen, Q.; Tripathy, M.; Luijten, E.; Schweizer, K. S.; Granick, S. Janus particle synthesis and assembly. *Adv. Mater.* **2010**, *22*, 1060−1071.

(12) Zhang, J.; Grzybowski, B. A.; Granick, S. Janus particle synthesis, assembly, and application. *Langmuir* **2017**, *33*, 6964−6977.

(13) Walther, A.; Müller, A. H. E. Janus particles: Synthesis, self-assembly, physical properties, and applications. *Chem. Rev.* **2013**, *113*, 5194−5261.

(14) Duan, Y.; Zhao, X.; Sun, M.; Hao, H. Research advances in the synthesis, application, assembly, and calculation of Janus materials. *Ind. Eng. Chem. Res.* **2021**, *60*, 1071−1095.

(15) Ge, L.; Cheng, J.; Sun, X.; Liu, J.; Wei, D.; Guo, R. Controlled group motion of anisotropic Janus droplets prepared by one-step vortex mixing. *ACS Appl. Mater. Interfaces* **2020**, *12*, 14588−14598.

(16) Zhang, Y.; Kang, L.; Huang, H.; Deng, J. Optically active Janus particles constructed by chiral helical polymers through emulsion polymerization combined with solvent evaporation-induced phase separation. *ACS Appl. Mater. Interfaces* **2020**, *12*, 6319−6327.

(17) Zhao, T.; Zhu, X.; Hung, C.-T.; Wang, P.; Elzatahry, A.; Al-Khalaf, A. A.; Hozzein, W. N.; Zhang, F.; Li, X.; Zhao, D. Spatial isolation of carbon and silica in a single Janus mesoporous nanoparticle with tunable amphiphilicity. *J. Am. Chem. Soc.* **2018**, *140*, 10009−10015.

(18) Smoukov, S. K.; Gangwal, S.; Marquez, M.; Velev, O. D. Reconfigurable responsive structures assembled from magnetic Janus particles. *Soft Matter* **2009**, *5*, 1285−1292.

(19) Erb, R. M.; Jenness, N. J.; Clark, R. L.; Yellen, B. B. Towards holonomic control of Janus particles in optomagnetic traps. *Adv. Mater.* **2009**, *21*, 4825−4829.

(20) Gibbs, J. G.; Zhao, Y.-P. Autonomously motile catalytic nanomotors by bubble propulsion. *Appl. Phys. Lett.* **2009**, *94*, 163104.

(21) Liu, F.; Li, Y.; Huang, Y.; Tsyrenova, A.; Miller, K.; Zhou, L.; Qin, H.; Jiang, S. Activation and assembly of plasmonic-magnetic nanosurfactants for encapsulation and triggered release. *Nano Lett.* **2020**, *20*, 8773−8780.

(22) Kang, C.; Honciuc, A. Influence of geometries on the assembly of snowman-shaped Janus nanoparticles. *ACS Nano* **2018**, *12*, 3741−3750.

(23) Yang, Z.; Wei, J.; Sobolev, Y. I.; Grzybowski, B. A. Systems of mechanized and reactive droplets powered by multi-responsive surfactants. *Nature* **2018**, *553*, 313−318.

(24) Liu, F.; Goyal, S.; Forrester, M.; Ma, T.; Miller, K.; Mansoorieh, Y.; Henjum, J.; Zhou, L.; Cochran, E.; Jiang, S. Self-assembly of Janus dumbbell nanocrystals and their enhanced surface plasmon resonance. *Nano Lett.* **2019**, *19*, 1587−1594.

(25) Silvera Batista, C. A.; Larson, R. G.; Kotov, N. A. Nonadditivity of nanoparticle interactions. *Science* **2015**, *350*, No. 1242477.

(26) Zhao, N.; Liu, K.; Greener, J.; Nie, Z.; Kumacheva, E. Close-packed superlattices of side-by-side assembled Au-CdSe nanorods. *Nano Lett.* **2009**, *9*, 3077−3081.

(27) Nie, Z.; Fava, D.; Kumacheva, E.; Zou, S.; Walker, G. C.; Rubinstein, M. Self-assembly of metal-polymer analogues of amphiphilic triblock copolymers. *Nat. Mater.* **2007**, *6*, 609−614.
(28) Parr, R. G.; Pearson, R. G. Absolute hardness: Companion parameter to absolute electronegativity. *J. Am. Chem. Soc.* **1983**, *105*, 7512−7516.
(29) Boles, M. A.; Ling, D.; Hyeon, T.; Talapin, D. V. The surface science of nanocrystals. *Nat. Mater.* **2016**, *15*, 141−153.
(30) Nag, A.; Kovalenko, M. V.; Lee, J.-S.; Liu, W.; Spokoyny, B.; Talapin, D. V. Metal-free inorganic ligands for colloidal nanocrystals: S^{2-}, HS^{-}, Se^{2-}, HSe^{-}, Te^{2-}, HTe^{-}, TeS_3^{2-}, OH^{-}, and NH_2^{-} as surface ligands. *J. Am. Chem. Soc.* **2011**, *133*, 10612−10620.
(31) Kovalenko, M. V.; Scheele, M.; Talapin, D. V. Colloidal nanocrystals with molecular metal chalcogenide surface ligands. *Science* **2009**, *324*, 1417−1420.
(32) Ban, H. W.; Park, S.; Jeong, H.; Gu, D. H.; Jo, S.; Park, S. H.; Park, J.; Son, J. S. Molybdenum and tungsten sulfide ligands for versatile functionalization of all-inorganic nanocrystals. *J. Phys. Chem. Lett.* **2016**, *7*, 3627−3635.
(33) Ban, H. W.; Oh, J. G.; Jo, S.; Jeong, H.; Gu, D. H.; Baek, S.; Lee, S. Y.; Park, Y. I.; Jang, J.; Son, J. S. Polyphosphide precursor for low-temperature solution-processed fibrous phosphorus thin films. *Chem. Mater.* **2019**, *31*, 5909−5918.
(34) Baek, S.; Kim, J.; Kim, H.; Park, S.; Ban, H. W.; Gu, D. H.; Jeong, H.; Kim, F.; Lee, J.; Jung, B. M.; Choa, Y.-H.; Kim, K. H.; Son, J. S. Controlled grafting of colloidal nanoparticles on graphene through tailored electrostatic interaction. *ACS Appl. Mater. Interfaces* **2019**, *11*, 11824−11833.
(35) Choi, W.; Kim, J. M.; Hwang, C.-K.; Choe, M.; Baek, S.; Ban, H. W.; Gu, D. H.; Jeong, H.; Chae, K. H.; Lim, Y.; Lee, Z.; Kim, J. Y.; Son, J. S. Thiometallate precursors for the synthesis of supported Pt and PtNi nanoparticle electrocatalysts: Size-focusing by S capping. *Nanoscale* **2020**, *12*, 10498−10504.
(36) Dong, Y.; Su, Y.; Hu, Y.; Li, H.; Xie, W. Ag_2S-CdS p-n nanojunction-enhanced photocatalytic oxidation of alcohols to aldehydes. *Small* **2020**, *16*, No. 2001529.
(37) Chai, Y.; Hasnain, J.; Bahl, K.; Wong, M.; Li, D.; Geissler, P.; Kim, P. Y.; Jiang, Y.; Gu, P.; Li, S.; Lei, D.; Helms, B. A.; Russel, T. P.; Ashby, P. D. Direct observation of nanoparticle-surfactant assembly and jamming at the water-oil interface. *Sci. Adv.* **2020**, *6*, No. eabb8675.
(38) Glaser, N.; Adams, D. J.; Böker, A.; Krausch, G. Janus particles at liquid-liquid interfaces. *Langmuir* **2006**, *22*, 5227−5229.
(39) Guzowski, J.; Korczyk, P. M.; Jakiela, S.; Garstecki, P. The structure and stability of multiple micro-droplets. *Soft Matter* **2012**, *8*, 7269−7278.
(40) Wei, D.; Ge, L.; Lu, S.; Li, J.; Guo, R. Janus particles templated by Janus emulsions and application as a pickering emulsifier. *Langmuir* **2017**, *33*, 5819−5828.
(41) Zhang, L.; Eisenberg, A. Thermodynamic vs kinetic aspects in the formation and morphological transitions of crew-cut aggregates produced by self-assembly of polystyrene-*b*-poly(acrylic acid) block copolymers in dilute solution. *Macromolecules* **1999**, *32*, 2239−2249.
(42) Discher, D. E.; Eisenberg, A. Polymer vesicles. *Science* **2002**, *297*, 967−973.
(43) Wilmes, G. M.; Durkee, D. A.; Balsara, N. P.; Liddle, J. A. Bending soft block copolymer nanostructures by lithographically directed assembly. *Macromolecules* **2006**, *39*, 2435−2437.
(44) Antonietti, M.; Förster, S. Vesicles and liposomes: A self-assembly principle beyond lipids. *Adv. Mater.* **2003**, *15*, 1323−1333.
(45) Chumpitaz, L. D. A.; Coutinho, L. F.; Meirelles, A. J. A. Surface tension of fatty acids and triglycerides. *J. Am. Oil Chem. Soc.* **1999**, *76*, 379−382.
(46) Wilk, K. A.; Syper, L.; Burczyk, B.; Sokolowski, A.; Domagalska, B. W. Synthesis and surface properties of new dicephalic saccharide-derived surfactants. *J. Surfactants Deterg.* **2000**, *3*, 185−192.
(47) Queimada, A. J.; Marrucho, I. M.; Coutinho, J. A. P. Surface tension of pure heavy n-alkanes: A corresponding states approach. *Fluid Phase Equilib.* **2001**, *183*, 229−238.

https://doi.org/10.1021/jacsau.2c00333
JACS Au 2022, 2, 2307−2315